npj | flexible electronics

Article

Published in partnership with Nanjing Tech University

https://doi.org/10.1038/s41528-025-00399-3

Waterproof and conductive tough fibers for washable e-textile

Hansu Kim[1,5], Jun-Gyu Choi[2,5], Taeyeon Oh[1], Inho Lee[1], Hyeongbeom Lee[1], Hanbit Jin[3], Chan-Hwa Hong[3], Hye Jin Kim[3] ✉, Tae-Wook Kim[4] ✉ & Sungjun Park[1,2] ✉

Conductive fibers are essential for wearable electronics, especially in electronic textiles (e-textiles) used as skin-interfaced sensors and interconnects. Achieving sustainable e-textiles with integrated toughness, waterproofing, and washability remains challenging. We present waterproof conductive tough fibers (CTFs) fabricated via a scalable, continuous capillary tube-assisted coating (CTAC) process. The multilayered CTFs demonstrate a conductivity of 6.42 kS/cm, Young's modulus of 6.22 MPa, toughness of 9.40×10^5 J/m^3, and 70% strain at break. With lengths exceeding 20 m, a native oxide layer on the eutectic gallium-indium (EGaIn) shell ensures reliable waterproofing with the IPX8 standard. They also maintain consistent performance for 24 days water immersion and repeated washing up to 100 cycles, showing superior resistance retention compared to the EGaIn-absence fibers. As a proof-of-concept, they enable wireless power transfer and reliable monitoring of electrocardiogram and electromyogram signals, establishing a robust platform for sustainable e-textiles.

Conductive fibers have emerged as pivotal innovations in wearable electronics, particularly in electronic textiles (e-textiles), by functioning as both sensors and electrical interconnectors[1–4]. Their seamless integration as one-dimensional electrodes into fabrics has driven advancements across diverse fields, including smart uniforms[5,6], human-machine interfaces[7,8], and non-invasive, real-time physiological signal monitoring[9,10], all without compromising mobility or comfort. The core of this technology lies in the development of conductive fibers that meet several key requirements[11–13]: (1) high conductivity, essential for capturing weak signals with minimal noise while ensuring power-efficient operation; (2) mechanical durability, ensuring toughness and/or tensile strength to resist mechanical deformations during wearing and movement, which can lead to inconsistent performance and cracks/scraps; (3) sustainability, enabling fibers to maintain their performance over prolonged use and repeated wash cycles; (4) uniformity, necessary for consistent sensing performance across extended lengths seamlessly integrated into fabrics; and (5) affordability, allowing for cost-effective mass production suitable for widespread consumer adoption.

From the perspective of materials and manufacturing processes, early developments in conductive fiber-based e-textiles primarily relied on fibers spun directly from individual composite materials, such as conducting polymers[14,15], nanostructured metals[16,17], and two-dimensional[18,19] or carbon materials[20,21]. While these approaches offered uniform electrical performance, ease of processing, and flexibility in structural modification, the single-material approach has suffered from limited stability against vigorous movement, strain, and moisture. Thus, multilayer structures have been proposed as more effective alternatives for e-textiles, which combine functional materials to improve their durability and functionality.

State-of-the-art multilayer fibers have enhanced the functionality of e-textiles by introducing advanced materials in each layer to meet specific requirements. One innovation involves an introduction of two distinct layers based on liquid metal particles, which were sequentially deposited on raw fiber substrate, achieving mechanical durability and stretchability up to 150% strain, while maintaining stable conductivity under deformation—as indicated by a low gauge factor of 0.1—and high conductivity exceeding 10 kS/cm for efficient signal transmission with minimal energy loss[22]. To address the limitation of liquid metal particles regarding scraps during wearing[23], poly(sodium 4-styrenesulfonate) was attached to stabilize the particles within the multilayer structure, thereby enhancing mechanical durability during repeated deformation. Similarly, polyester yarn was coated in multi-walled carbon nanotubes (MWCNTs) dispersion with polymer resins, forming a multilayer structure that improves mechanical strength and electrical conductivity[24]. An annealing process strengthens the interaction between the MWCNT shell and polyester core, achieving extremely high tensile strength up to 260 MPa with 25% of elongation limit. Recent

[1]Department of Intelligence Semiconductor Engineering, Ajou University, Suwon, Republic of Korea. [2]Department of Electrical and Computer Engineering, Ajou University, Suwon, Republic of Korea. [3]Intelligent Components and Sensors Research Section, Electronics and Telecommunications Research Institute (ETRI), Daejeon, Republic of Korea. [4]Department of Flexible and Printable Electronics, Jeonbuk National University, Jeonju, Republic of Korea. [5]These authors contributed equally: Hansu Kim, Jun-Gyu Choi. ✉e-mail: nolawara@etri.re.kr; twk@jbnu.ac.kr; sj0223park@ajou.ac.kr

studies have also leveraged interlocking structures using MXene, such as hierarchically interlocked helical configurations[25] or core-sheath heterogeneous designs[26], to achieve exceptional conductivity exceeding 10^3 S/cm and mechanical stretchability under large deformations up to 300%. Furthermore, hydrogel-coated fibers offered remarkable environmental stability[27]. Inspired by spider silk, a coating of polyacrylic acid sodium hydrogel enabled maintenance of conductivity even at extremely low temperatures (retaining conductivity down to −35 °C) and provided rapid recovery rate within large strains (fast resilience within 30 s from stretching up to 1200%). Substantial efforts have been devoted to achieving the desired characteristics of conductive fibers through the integration of multilayer structures, with an emphasis on addressing specific performance requirements.

However, despite these advancements, the development of sustainable fibers for practical use in e-textiles remains challenging due to issues with toughness, waterproofing, and washability. Conductive fibers often struggle to maintain stable performance in response to external factors such as repeated stretching, scratching, sweat, wet weather, and washing. Liquid metals, while used as particle-embedded matrices, are limited by their vulnerability to friction during continuous deposition. While advanced carbon materials offer exceptional toughness, they are prone to environment-induced chemical degradation, with prolonged exposure to moisture or oxygen leading to performance loss. Mechanically flexible and strong hydrogels, on the other hand, lose their functionality when exposed to laundry detergents acting as surfactants. Therefore, innovative strategies should be developed for conductive fibers that simultaneously meet these requirements, creating high-performance e-textiles capable of daily, practical, and sustainable use.

In this study, we present waterproof conductive tough fibers (CTFs) fabricated using a scalable, continuous capillary tube-assisted coating (CTAC) process, addressing key challenges in e-textile development. The three-layer configuration was strategically designed to synergize mechanical resilience, electrical conductivity, and waterproof performance within a single fiber platform. The CTFs feature a multilayer structure with each layer serving a critical role: a stretchable polyester-rayon core provides a durable and flexible foundation; an Ag flake–waterborne polyurethane (AF–WPU) composite middle layer enhances mechanical stability, electrical conductivity, and interfacial adhesion; and an outer eutectic gallium-indium (EGaIn) shell delivers exceptional conductivity. This design achieves high conductivity of 6.42 kS/cm, Young's modulus of 6.22 MPa, toughness of 9.40×10^5 J/m^3, and a strain at break of 70%. The rapid formation of a native oxide layer on the EGaIn shell imparts exceptional waterproofing, enabling the fibers to meet IPX8 waterproofing standards. Additionally, the CTAC process allows scalable fabrication of fibers over 20 m long. These long CTFs retained their electrical performance and original shape after 24 days of immersion under IPX8-standard conditions and multiple washing cycles. As a proof-of-concept, the CTFs powered wireless energy transfer via electromagnetic induction and demonstrated reliable monitoring of electrocardiogram (ECG) and electromyogram (EMG) signals with a signal-to-noise ratio of 40.3 dB, even after extensive washing and wet exposure. This work establishes a robust and scalable platform for creating sustainable e-textiles with reliable performance in demanding real-world applications.

Results and discussion

Continuous manufacturing of multilayered conductive tough fibers

Figure 1a illustrates the overall process for manufacturing multilayered CTFs and their component materials. As a promising strategy for the continuous fabrication of multilayered fibers, we exploited capillary action within a confined tube with 1-mm-inner diameter to uniformly coat fibers, enabling precise control over layer thickness and material distribution. This process, referred to as the CTAC process, allowed for the formation of well-defined microfibers with a core–shell structure. Unlike the conventional coating processes for multilayered fibers, typically utilizing bulk bath for dipping[28], the CTAC process is significantly waste-efficient, requiring a very small amount of solution (~70 μL) per cycle.

The polyester-rayon synthetic fiber, used as the core of CTFs, exhibited a tensile strength of 3.58 gf/denier[29], demonstrating its role as a tough and durable framework. A conductive filler matrix composed of AF and WPU was deposited onto the raw fibers during the first CTAC process. WPU, formulated with an environmentally friendly water-based solvent[30], ensures robust adhesion to the raw fiber through favorable interactions[31,32]. Simultaneously, the metallic AF increases the surface energy of filler layer, facilitating the effective attachment of the EGaIn shell. Note that optimizing the composition ratio is crucial for achieving the appropriate viscosity for the filler matrix. Excessive AF concentrations result in overhardened suspensions, whereas excessive WPU concentrations produce overdiluted suspensions (Supplementary Fig. 1), both of which disrupt the CTAC process. After drying the filler layer, EGaIn was continuously deposited as a secondary layer using the CTAC process, yielding an ultra-conductive microfiber. Unlike conventional solid metals, the fluidic properties of EGaIn enable facile deformation and strong coating capability. The superior conductivity and mechanical toughness of the CTFs developed in this study are remarkable compared to those of recently reported conductive fibers fabricated from various materials (Fig. 1b)[27,33–41] and the figure-of-merit parameters of these fibers are summarized in Supplementary Table 1.

Figure 1c illustrates interfacial adhesion on fibers and their step-by-step fabrication process using the CTAC process. Each process involves three main steps with the following principles. (1) A well-blended conductive filler suspension is dropped at the entrance of a tube with a 1-mm inner diameter, while the raw fiber is threaded through, forming a meniscus of the filler suspension between the rounded tube edge and the raw fiber. The meniscus is automatically drawn into the tube via capillary action. Considering the composition of anionic aliphatic WPU[42,43], employed in this work, hydrophobic (polyol, isocyanate) groups of the filler suspension facilitates better spreading and wetting on the hydrophobic polyester-rayon fibers. This ensures a uniform and adherent coating with an increased interaction area. (2) The suspension meniscus is then drawn deeply into the tube by continuous injection. During the suspension flow, the constant injection ensures uniform coating thickness by filling the textured surface of the raw fiber (Supplementary Fig. 2), while the injection speed determines the thickness of the coating[44]. At relatively low injection speeds, the thickness of the shell layer is primarily governed by capillary action. Faster flow provides insufficient time for interaction between suspension and underlying fiber, thus resulting in a thinner layer due to evaporation. Conversely, beyond the critical speed with a minimum thickness, a shear force within the suspension, referred to as viscous drag. Rapidly flowing suspension leaves more fluids due to increased viscous drag, which turns in thicker layer, as interpreted by the Landau-Levich model[45,46]. Therefore, understanding the relationship between injection speed and layer thickness is essential to achieving the desired thickness in the CTAC process. (3) Finally, the volatile solvent in the filler matrix is rapidly evaporated using a drier as the fiber exited the tube, resulting in a densification (i.e., hardening).

With the same manner, the CTAC process is repeated with EGaIn, replacing the filler suspension. A key difference lies in the necessity of the filler matrix for successful EGaIn coating. Supplementary Fig. 3 and Supplementary Video 1 present time-lapse images and videos of raw fibers and filler-coated fibers being gradually pulled upward from EGaIn droplets, highlighting the critical role of metallic AF in increasing the surface energy of the middle layer to facilitate EGaIn adhesion. Additionally, subsequent drying enables native oxidation of EGaIn, forming an oxide layer that functions as a passivation layer. Consequently, the fabricated CTFs demonstrate enhanced mechanical durability and toughness, with minimized abrasion-induced cracks (Supplementary Fig. 4)

Morphological, chemical, and mechanical analysis of CTFs

Figure 2a presents optical microscopy (OM) and scanning electron microscopy (SEM) images of the fibers at different stages, showing the side and cross-sectional views, respectively. These images demonstrate the

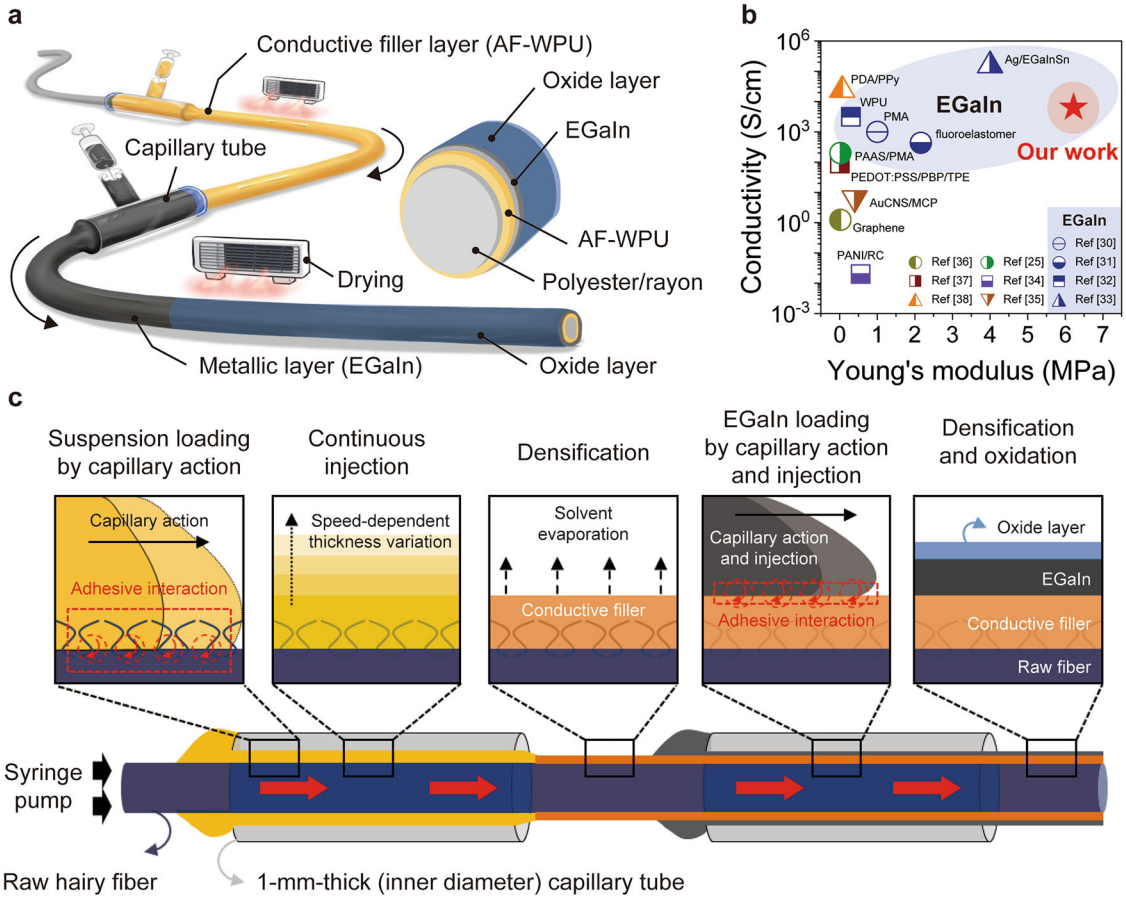

Fig. 1 | Capillary tube-assisted coating (CTAC) process for manufacturing conductive tough fibers (CTFs). a Schematic of manufacturing process for CTFs using the CTAC method (inset box), showing the components of the CTFs. **b** Comparison of the conductivity and Young's modulus of the CTF with those of previously reported conductive fibers. **c** Schematic illustrating the overall CTAC process for transforming raw fibers into multilayer-structured CTFs.

morphological evolution during the double CTAC process. The raw fibers, composed of spiral bundles of discrete fibers, exhibited hairy and non-uniform surfaces. However, the subsequent coating of filler matrix effectively covered the rough surfaces, attributed to the enhanced wettability by hydrophobic interactions. This leads to a relatively smooth surface. And then, the second CTAC process with EGaIn yielded a well-defined core-shell structured CTF. Figure 2b shows the cross-sectional SEM and energy dispersive spectroscopy (EDS) mapping images of the CTF, highlighting the elemental distributions of (i) C K, (ii) Ag L, (iii) In L, and (iv) Ga L series. Both the filler matrix and EGaIn layers were processed using the CTAC method at a fixed speed of 20 mm/min. The black craters observed in the Ag L and C K series correspond to raw fibers, where the elemental information represents AF and WPU, respectively. Since the relatively heavy AF particles are localized in the fiber core, the exposed WPU is more susceptible to water-induced swelling, necessitating the subsequent EGaIn coating. Consequently, the EGaIn layer, as clearly observed in the images, was successfully deposited with a thickness of around 63 μm.

Further investigation into the chemical composition of the CTF was conducted using X-ray photoelectron spectroscopy (XPS) analysis. Depth-dependent chemical analysis was performed via continuous scanning and repeated in situ etching with Ar gas. Figure 2c shows the relative atomic distributions of C, O, Ga, and Ag a function of etching depth, with all peaks normalized to a reference peak for physisorbed CO_2 (Supplementary Fig. 5). The relative concentrations of O and Ga decreased with increasing etching depth, whereas those of C and Ag increased. Since the outermost layer is EGaIn, the high O content at the surface level corresponds to native oxides acting as passivation layers. Notably, the depth-profiled XPS spectra for each atomic orbital are shown in Fig. 2d–f. The background level of the O 1 *s* spectra decreased significantly after a single etching step, indicating the successful removal of native oxide layer originating from EGaIn. At the surface level, the O 1 *s* spectra exhibited two distinct peaks at 532.8 eV and 531.7 eV, denoted as O (i) and O (ii), respectively. The O (i) peak corresponds to deeper levels and is attributed to O species involved in the polymer backbone of WPU and/or the raw fiber. As higher binding energies reflect bonding with more electronegative atoms of lower quantum numbers, the O (ii) peak, observed exclusively at the surface, represents native oxides. Consistently, the Ga $2p_{3/2}$ spectra confirmed the native oxidation of the outermost EGaIn, as evidenced by two distinct peaks at 1118.6 eV and 1116.2 eV, corresponding to oxidized Ga_2O_3 and metallic Ga, respectively[47]. Meanwhile, the peak intensities in the Ag 3 *d* spectra increased with etching depth, indicting proximity to the AF layer deeper within the structure. These spectra also showed double peaks resulting from spin-orbital splitting[48]. Collectively, these comprehensive analyses validate the well-defined core-shell structure of the CTF.

To validate the capability of each fiber as an e-textile, we investigated their electrical and mechanical properties. Figure 2g shows the fiber thickness at varying CTAC speeds from 10 to 40 mm/min. As discussed earlier, the injection speed during the CTAC process determines the thickness of layers. Specifically, the selected injection speeds belong to the regime governed by viscous drag, thus slower injection was advantageous for enhancing electrical conductivity (Fig. 2h). While the coating thickness can be lowered to enhance the conductivity, excessively slow injection rates restrict scalable fabrication. Therefore, the injection speed was set at 20 mm/min. The resulting diameter and conductivity of the fibers coated with the filler matrix were 232 μm and 307 S/cm, respectively, whereas those of CTFs were 295 μm and 6.42 kS/cm. Additionally, the CTFs demonstrated enhanced

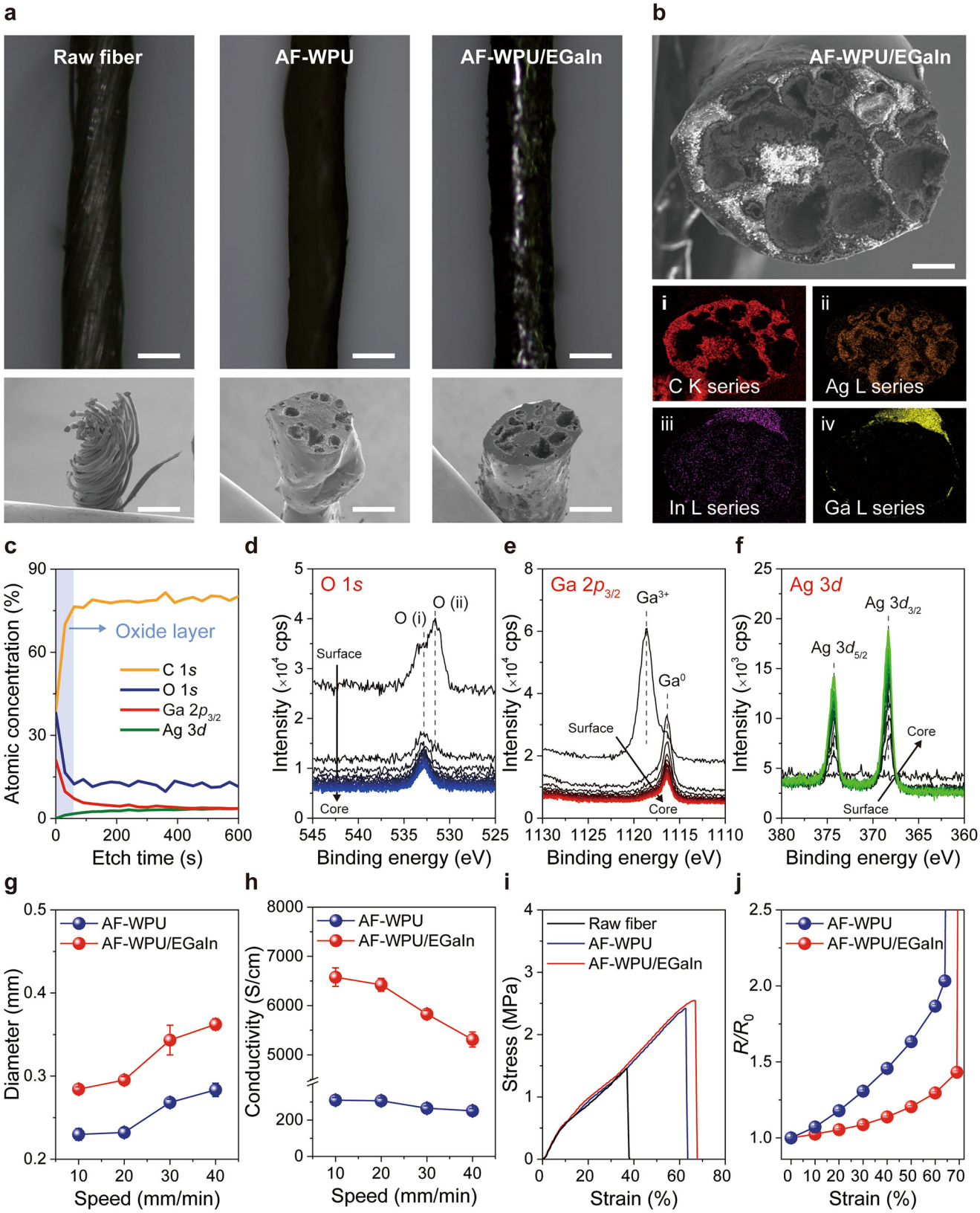

Fig. 2 | Electrical and mechanical characteristics of CTFs. a OM and SEM images of raw fibers, filler matrix-coated fibers, and CTFs. Each scale bar in microscopic image denotes 200 nm. **b** Cross-sectional SEM images of the CTF with EDS mapping for (i) C K, (ii) Ag L, (iii) In L, and (iv) Ga L series. Each scale bar in microscopic image denotes 50 nm. **c** Relative atomic distributions of the CTF obtained through XPS depth-profiling analyses. The XPS spectra of the CTF from surface to core levels correspond to **d** O 1 *s*, **e** Ga $2p_{3/2}$, and **f** Ag 3 *d* orbitals. **g** Diameter and **h** electrical conductivity of each fiber as functions of the CTAC process speed. **i** Strain-stress curves for each fiber. **j** Relative resistance changes of each fiber as a function of strain.

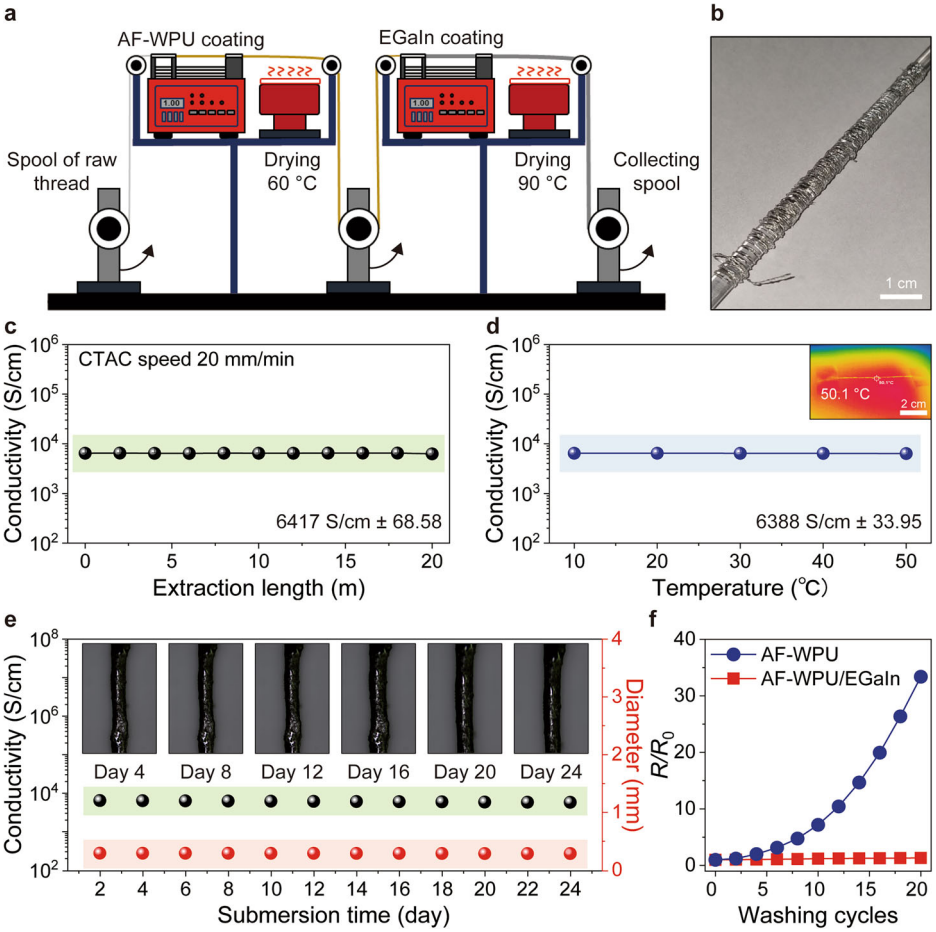

Fig. 3 | Scalable manufacturing of crack-free waterproof CTFs. a Schematic of the large-area coating process for the CTFs, including the CTAC and immediate drying. **b** Schematic of the large-area coated CTF wound around a glass rod. **c** Consistent electrical conductivity of a 20 m CTF, demonstrating stability in large-area manufacturing. **d** Heat resistance of the CTFs, showing reliable performance at 50.1 °C, suitable for practical use in daily life. **e** Changes in diameter and electrical conductivity of the CTFs after 24 days of water immersion, demonstrating the retention of both properties. The waterproof test was performed under IPX8 standard conditions. **f** Relative resistance changes of each fiber over washing cycle, with each cycle lasting 10 min.

mechanical strength (Fig. 2i). Notably, the additional layer deposition for the core-shell structure subtly adjusted the rigidity and elasticity[49]. The CTFs exhibited a breakdown stress of 2.54 MPa, a strain of 70%, Young's modulus of 6.22 MPa, toughness of 9.40×10^5 J/m^3, all while maintaining ultrahigh conductivity. The CTFs also exhibited reduced changes in conductivity under mechanical deformation, as evaluated by the relative resistance (R/R_0) as a function of strain (Fig. 2j). Under 70% strain, the R/R_0 value of CTFs was 1.43, compared to 2.03 for AF-WPU fibers without the EGaIn layer, indicating that the EGaIn shell mitigated strain-induced conductivity instability. To assess the electro-mechanical cycle reliability of the CTFs, the relative changes in resistance and length values were recorded over 1000 cycles of tensile strain at 10–40% (Supplementary Figs. 6 and 7). The CTFs demonstrate complete resilience, maintaining a consistent relative length ($L/L_0 = 1$) after 1000 cycles of tensile strain, along with stable electrical performance with minimal resistance variation at strain levels up to 10%. While resistance variations increase under multiple cycles of larger strains, the CTF connected to an LED successfully functioned as an electrical conductor, maintaining stable performance despite repeated bending and stretching up to 70% strain (Supplementary Video 2), thereby demonstrating both mechanical durability and consistent electrical conductivity under deformation.

Scalable production and environmental stability of CTFs

The primary advantage of fiber-based electronics lies in their suitability for mass production. Leveraging the uniformity of the CTAC process, a large-scale roll-to-roll manufacturing system was designed, as shown in Fig. 3a. To minimize gravitational effects, the fiber was maintained in a horizontal orientation during the double CTAC process. Instantaneous drying of the filler matrix and EGaIn layers was achieved at controlled temperatures. Figure 3b displays the resulting thread wound around the glass stick, extending over 20 m in length. Despite vigorous winding, the thread showed no significant cracks or damage due to the robust surface provided by the EGaIn coating. Additionally, the conductivity of a long CTF produced at a CTAC speed of 20 mm/min was measured at 2 m intervals along its entire length (Fig. 3c), confirming uniform conductivity throughout the fiber. To further assess the suitability of the CTFs for skin-compatible e-textiles, we examined their temperature-dependent conductivity over a 20 m length (Fig. 3d). Given that the temperature of textiles in contact with human skin can fluctuate in daily use, the conductivity stability across a range of temperatures is critical for practical applications. The temperature of the CTF was recorded using an infrared camera (inset). Remarkably, the CTFs exhibited nearly constant conductivity across temperatures from 10 to 50 °C, underscoring their potential for integration into e-textiles. In comparison, fibers without the EGaIn layer displayed consistent but lower conductivity levels (Supplementary Fig. 8).

Waterproofing is a critical requirement for the sustainable use of e-textiles. To evaluate the waterproof capabilities of the CTFs, we conducted immersion tests based on the IPX8 standard, which involves continuous immersion in water beyond 1 m depth. Specifically, long CTFs were submerged in water at a depth of 1.5 m for up to 24 days, simulating extreme waterproofing conditions. Figure 3e illustrates the changes in conductivity and diameter of the CTF after this prolonged immersion. The long CTFs were meticulously tested to validate the reliability of the CTAC process for mass production, showing no significant cracks or damage. The native oxide on the outer shell protects against swelling of the filler matrix, allowing the non-hygroscopic CTFs to retain their conductivity and diameter. Crystallographic analysis further validated the absence of unexpected shell corrosion during long-term water immersion[50,51], as no additional diffraction

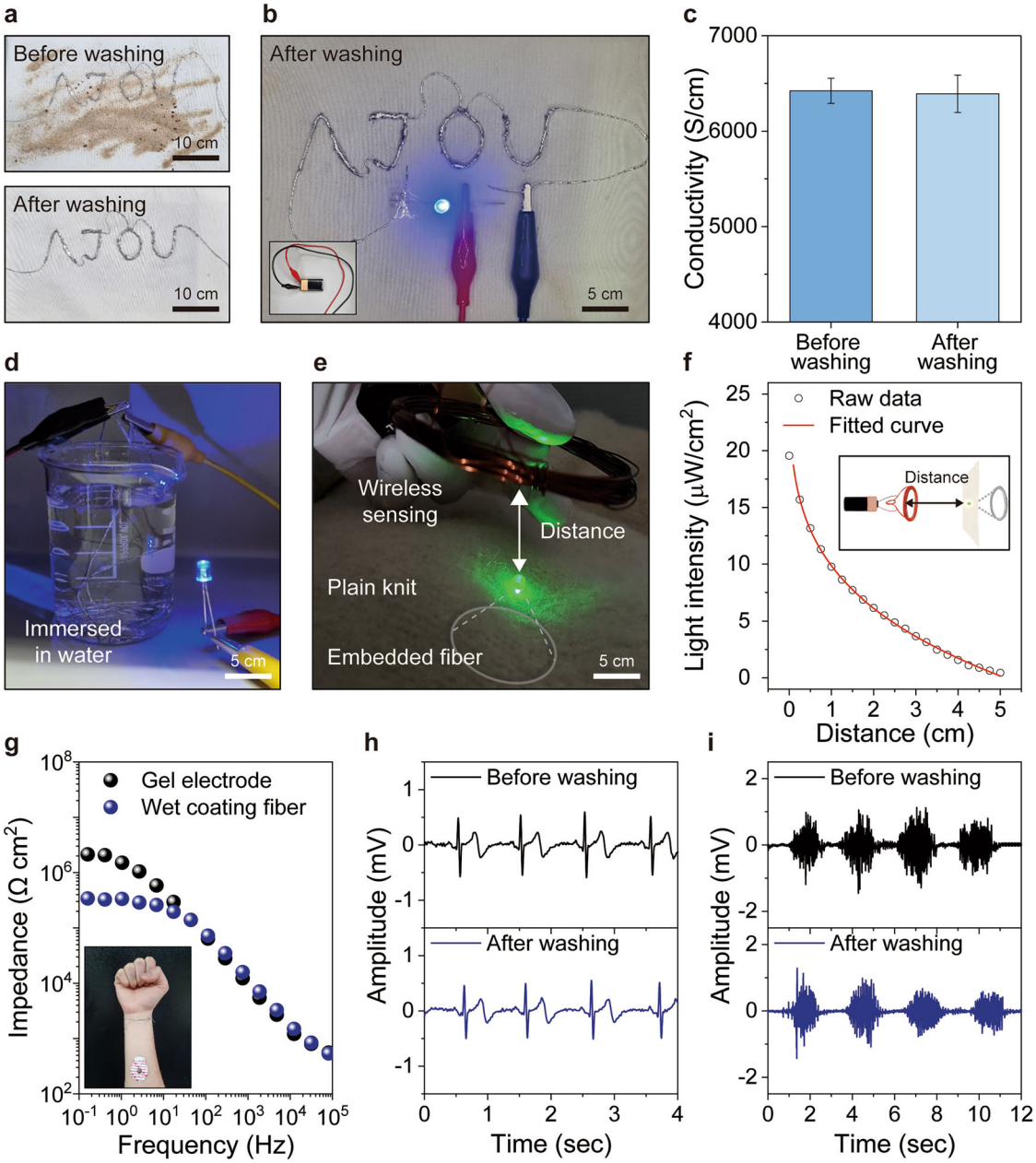

Fig. 4 | Sustainable washing and versatile applications of CTFs. a Schematic of the CTF washing process. **b** Schematic of an LED connected to the CTFs after the washing process, powered by a 9 V battery. **c** Electrical conductivity before and after washing, indicating minimal change due to their waterproof properties. **d** LED operation test with CTFs immersed in water. **e** Wireless power sensing experiment with a CTF wound under a knit on one side and copper wire on the other side, and **f** LED brightness as a function of the sensing distance. **g** Comparison of impedance between the gel electrodes and wet CTFs, thereby showing the impedance values ($<10^6$ Ω cm^2). **h** ECG and **i** EMG measurements using the CTFs before and after washing.

peaks attributable to phases other than native oxides were detected (Supplementary Fig. 9). Additionally, the inset OM images reveal no visible deformation or damage, even after prolonged immersion, highlighting the excellent waterproof capability of the CTFs in accordance with the IPX8 standard. Beyond waterproofing, washability is another crucial factor for the sustainable use of e-textiles. Figure 3f presents the relative resistance changes of AF-WPU-coated fibers and CTFs as a function of washing cycles, where a 20 m fiber was tightly wound on a slide glass for testing. Washability was evaluated in a stirring water bath, as demonstrated in Supplementary Video 3. While AF-WPU-coated fibers showed a significant increase in resistance after only a few washing cycles, the relative resistance difference ($\Delta R/R_0$) of the CTFs was 100 times lower than those for AF–WPU-coated fibers after 20 cycles. Notably, the $\Delta R/R_0$ of the CTFs demonstrated negligible changes of resistance (Supplementary Fig. 10) and mechanical strength (Supplementary Fig. 11), even after 100 washing cycles. This remarkable washability can be attributed to the native oxide layer of EGaIn, which provides effective protection against mechanical stress and water ingress during washing. Consequently, the CTFs exhibit not only exceptional waterproof properties but also maintain stable electrical performance after repeated washing, reinforcing their potential for practical e-textile applications.

Sustainable washing and versatile applications of CTFs

To evaluate the feasibility of integrating CTFs into e-textiles, they were sewn onto commercial cotton. Figure 4a shows the washability test of the CTF-sewn cotton after rigorous washing. Despite minor scratching from the millimeter-sized dirt particles, the sewn CTF functioned as electric wire, powering an LED (Fig. 4b) and maintaining conductivity after laundering

(Fig. 4c). While tightly wound raw fibers absorbed various liquids such as deionized (DI) water, milk, orange juice, wine, and coffee within 30 min (Supplementary Fig. 12), the CTFs demonstrated no significant liquid absorption even after 120 min (Supplementary Fig. 13). When stained with colored ink, the CTFs were effectively cleaned with DI water, further confirming their ability to power an LED after washing (Supplementary Video 4). The CTFs also demonstrated electrical functionality underwater, as shown in Fig. 4d and Supplementary Fig. 14. As demonstrated in Supplementary Video 5, the LED connected to the submerged CTFs remained lit during vigorous mechanical deformations such as bending and stretching up to 70% strain. This observation underscores the waterproof and mechanically robust properties of the CTFs in wet environments, further validating their suitability for practical e-textile applications.

Beyond waterproof functionality, coiled CTFs enabled wireless powering via electromagnetic induction. Figure 4e displays the experimental setup, comprising a transmitter with a Cu enamel coil and a receptor with a knit-sewn CTF coil. A negative-positive-negative (NPN) transistor and resistor units connected to the enamel coil and a commercial battery facilitated the conversion of direct current (DC) into alternating current (AC) in the transmitter. The detailed circuit diagram is shown in Supplementary Fig. 15. The AC power generated alternating magnetic fields that wirelessly powered an LED connected to the CTF coil in the receptor. Figure 4f shows the light intensities of the LED as a function of the distance between the transmitter and receptor, following the power-law of light intensity[52].

Another wearable application of the CTFs is as physiological signal sensors. The CTF-based electrode demonstrated impedance levels comparable to gel electrodes across the frequency ranges relevant to physiological signals, including ECG (~20 Hz)[49] and EMG (~100 Hz)[50], even under wet conditions (Fig. 4g). This performance addresses the limitations of gel electrodes, which can cause skin irritation during prolonged use and are less suitable for extended monitoring. The comparable impedance of the CTF-based electrode highlights its potential as a practical alternative to commercial gel electrodes for physiological signal detection. Figures 4h, i display the ECG and EMG signals before and after laundering, respectively, demonstrating consistent signal integrity. CTFs exhibit a range of promising features, including crack-free durability, ultrahigh conductivity, scalability for mass production, temperature-stability, washability, and suitability as skin-compatible electrodes for physiological signal monitoring. These attributes underscore their potential for advancing fabric-based e-textiles through large-scale manufacturing, paving the way for innovations in smart clothing technology.

Discussion

In conclusion, this study successfully develops sustainable e-textiles based on waterproof conductive tough fibers (CTFs) with a multilayer AF–WPU/EGaIn structure, ensuring high conductivity and mechanical toughness. The rapid in-situ formation of a native oxide layer on the EGaIn shell provides exceptional waterproofing, enabling the fibers to exceed IPX8 standards and operate reliably under submerged conditions. Additionally, the scalable CTAC process allows the extended and uniform fibers of which length exceeds 20 m. They also maintain consistent electrical and mechanical properties even after multiple washing, underwater deformation, and ink contamination. These fibers demonstrate robust performance in wireless power transfer and physiological signal sensing, including ECG and EMG signals, even in wet conditions. The low-noise measurements after laundering emphasize their potential for non-invasive health monitoring. These advancements establish a new benchmark for durable, functional, and scalable e-textiles, paving the way for smart clothing and wearable technologies that can withstand demanding environments.

Methods

Preparation of inner and outer shell coating materials

Initially, 1.0 g of AFs (>99.99%, Daejoo Electronic Materials Co., Ltd.) was combined with 1.5 g of WPU (solids content 59.5–61.5%, Alberdingk Boley Co., Ltd.) at room temperature and vigorously stirred by vortex mixer for 30 min. The CTAC process was later conducted by injecting the mixture at a speed of 20 mm/min into a polyester-rayon synthetic raw fiber connected to the syringe pump. After the initial coating, the fiber was dried on a 60 °C dryer for 10 min to ensure proper adhesion properties. Finally, EGaIn (75.5 wt% Ga and 24.5 wt% In, MSE Supplies) was applied using the CTAC process as previously described. The fully coated fiber was dried in a 90 °C dryer for over 30 min. This process was repeated for mass production of CTFs.

Capillary tube-assisted coating (CTAC) method

The micro hematocrit capillary tube (70 μL of capacity, 1.1 mm of inner diameter, 0.20 mm of wall thickness, and 75 mm of length, Korea Ace Scientific) was used in the CTAC process. It was positioned at the center of a syringe pump (NE-1010, New Era Pump Systems, Inc.). The fibers were passed through the fixed capillary tube, while the coating agent was injected at a speed of 20 mm/min, as set on the syringe pump to 20 mm/min. The syringe pump facilitated the coating process[44].

Electrical and mechanical measurement

We assessed the sheet resistance of the CTF using the four-point probe (4pp) method (HPS2663, Helpass Electronic Technologies, Inc.). To ensure optimal alignment between the sample size and 4pp tips, the probe spacing was set to 2 mm. Tensile measurements were conducted using a universal testing machine (UTM) (LDW-5, Jinan Chuanbai Instrument Equipment Co., Ltd.), with a load cell of 20 N, where the length of CTF samples was fixed at 6 cm. Uniaxial strain was applied at a rate of 20 mm/min, while the load cell was calibrated prior to testing. Both electrical and mechanical measurements were conducted at room temperature.

XPS measurements

The chemical compositions of the layered structure of AF–WPU with EGaIn were analyzed using X-ray photoelectron spectroscopy (XPS-NEXSA, Thermo Fisher Scientific) with a monochromated Al Kα source. Depth-profiling was conducted via repeated etching using an Ar gas flow, with scans conducted at intervals of 30 s.

Immersion testing procedure for CTFs according to IPX8 standard

The waterproof capability of the CTFs was evaluated by conducting immersion tests under IPX8 standard conditions. The CTFs were completely submerged in a bath filled with DI water at a depth of 1.5 m, with the water temperature maintained at 20 °C to simulate typical environmental conditions. The immersion duration was set for up to 24 days to assess the long-term waterproof capability of the CTFs under prolonged exposure. After the designated immersion periods, the CTFs were carefully retrieved from the water for subsequent analyses, including measurements of conductivity, diameter, and visual inspections.

Submersion and washing procedures for CTFs in sewn textiles

The CTF was completely submerged in a bath filled with DI water to assess its long-term waterproof characteristics. For verifying a sustainability regarding washing capability, the CTFs, contaminated with sand, dust, and other debris, were washed for 1 h using a solution consisting of 30 g of commercial liquid laundry detergent (Frosch, Erdal Rex GmbH), where the temperature was fixed at 20 °C, as reported in previous research[53].

Wireless power transmission test using CTFs

A wireless power transmission test generates an induced current in the coil via electromagnetic induction. An enamel-copper wire coil was prepared by winding it more than 30 times, with a loop created in the middle of the coil. At both ends and loops of the coil, a 2N2222A transistor and 9.0 V battery were connected. On the other side, the developed CTF was wounded more than 30 times around the coil and connected to a LED. Here, the induced current increases as the distance between the two coils decreases.

Impedance measurement

Electrode-skin impedance measurements were conducted using an electrochemical workstation (CS350, Wuhan Corrtest Instruments Co., Ltd.) over a frequency range of 10^{-1}–10^{5} Hz. A sinusoidal stimulation voltage varying from 1 to 2500 mV was applied to obtain the impedance curve. The wet-coated CTF was wrapped around the right wrist. For comparison, Ag/AgCl electrodes (3 M Monitoring Electrode 2223H) were used to measure impedance under similar conditions, with each electrode having a surface contact area of 1.5×1.5 cm^2.

Physiological signal measurement with CTFs

Physiological signals were measured using CTFs, with ECG and EMG signals collected using an electrocardiography meter (1800; A-M systems microelectrode AC amplifier). Regarding the ECG measurements, the CTFs were configured as bracelets worn, a reference electrode placed on the forearm. The electrodes were connected to a signal recording setting and processed using a bandpass filter (1–150 Hz). Regarding the EMG test, the CTFs were also worn as bracelets on the wrist to detect muscle signals from the biceps or brachial regions. Additionally, normal data were analyzed from clinical datasets obtained in a clinical setting with Institutional Review Board (IRB) approval (IRB Approval No. AJOU 202410-HB-003). All the data were processed and analyzed using the Matlab envelope function[54–56].

Data availability

All data are available within the article or available from the authors upon reasonable request.

Received: 30 November 2024; Accepted: 17 March 2025;
Published online: 31 March 2025

References

1. Lin, R. et al. Digitally-embroidered liquid metal electronic textiles for wearable wireless systems. *Nat. Commun.* **13**, 2190 (2022).
2. Hwang, S. et al. Integration of multiple electronic components on a microfibre towards an emerging electronic textile platform. *Nat. Commun.* **13**, 3173 (2022).
3. Torres Alonso, E. et al. Graphene electronic fibres with touch-sensing and light-emitting functionalities for smart textiles. *npj Flex. Electron* **2**, 1–6 (2018).
4. Kim, J., Campbell, A. S., de Ávila, B. E.-F. & Wang, J. Wearable biosensors for healthcare monitoring. *Nat. Biotechnol.* **37**, 389–406 (2019).
5. Wicaksono, I. et al. A tailored, electronic textile conformable suit for large-scale spatiotemporal physiological sensing in vivo. *npj Flex. Electron* **4**, 1–13 (2020).
6. Libanori, A., Chen, G., Zhao, X., Zhou, Y. & Chen, J. Smart textiles for personalized healthcare. *Nat. Electron* **5**, 142–156 (2022).
7. Luo, Y. et al. Learning human–environment interactions using conformal tactile textiles. *Nat. Electron* **4**, 193–201 (2021).
8. Yin, L. et al. A self-sustainable wearable multi-modular e-textile bioenergy microgrid system. *Nat. Commun.* **12**, 1542 (2021).
9. Phan, P. T. et al. Smart textiles using fluid-driven artificial muscle fibers. *Sci. Rep.* **12**, 11067 (2022).
10. Yin, J. et al. Smart textiles for self-powered biomonitoring. *Med-X* **1**, 3 (2023).
11. Montazeri Ghahjaverstan, N. et al. Textile-based wearable to monitor heart activity in paediatric population: a pilot study. *CJC Pediatr. Congenit. Heart Dis.* **2**, 187–195 (2023).
12. Zhou, B., Sundholm, M., Cheng, J., Cruz, H. & Lukowicz, P. Measuring muscle activities during gym exercises with textile pressure mapping sensors. *Pervasive Mob. Comput.* **38**, 331–345 (2017).
13. Lin, S. et al. Triboelectric micro-flexure-sensitive fiber electronics. *Nat. Commun.* **15**, 2374 (2024).
14. Liu, L., Chen, J., Liang, L., Deng, L. & Chen, G. A. PEDOT:PSS thermoelectric fiber generator. *Nano Energy* **102**, 107678 (2022).
15. Gao, C. et al. Continuous dry–wet spinning of white, stretchable, and conductive fibers of poly(3-hydroxybutyrate-co-4-hydroxybutyrate) and ATO@TiO2 nanoparticles for wearable e-textiles. *J. Mater. Chem. C.* **8**, 8362–8367 (2020).
16. Zhou, T. et al. Ultra-compact MXene fibers by continuous and controllable synergy of interfacial interactions and thermal drawing-induced stresses. *Nat. Commun.* **13**, 4564 (2022).
17. Chen, X. et al. A review on recent advancement of nano-structured-fiber-based metal-air batteries and future perspective. *Renew. Sustain. Energy Rev.* **134**, 110085 (2020).
18. Wan, J. et al. A universal construction of robust interface between 2D conductive polymer and cellulose for textile supercapacitor. *Carbohydr. Polym.* **284**, 119230 (2022).
19. Zhao, Y. et al. All-fiber structure covered with two-dimensional conductive MOF materials to construct a comfortable, breathable and high-quality self-powered wearable sensor system. *J. Mater. Chem. A* **10**, 1248–1256 (2022).
20. Ming, X. et al. 2D-Topology-seeded graphitization for highly thermally conductive carbon fibers. *Adv. Mater.* **34**, 2201867 (2022).
21. Gelfond, J., Meng, T., Li, S., Li, T. & Hu, L. Highly electrically conductive biomass-derived carbon fibers for permanent carbon sequestration. *Sustain. Mater. Technol.* **35**, e00573 (2023).
22. Lee, G.-H. et al. Conductance stable and mechanically durable bi-layer EGaIn composite-coated stretchable fiber for 1D bioelectronics. *Nat. Commun.* **14**, 4173 (2023).
23. Huang, K. et al. An anti-leakage liquid metal thermal interface material. *RSC Adv.* **10**, 18824–18829 (2020).
24. Ma, L. et al. Preparation of core/shell electrically conductive fibers by efficient coating carbon nanotubes on polyester. *Adv. Fiber Mater.* **3**, 180–191 (2021).
25. Zhang, W. et al. Hierarchically interlocked helical conductive yarn enables ultra-stretchable electronics and smart fabrics. *Chem. Eng. J.* **462**, 142279 (2023).
26. Hou, Z. et al. Core–sheath heterogenous interlocked stretchable conductive fiber induced by adhesive MXene modulated interfacial soldering. *Nano Lett.* **24**, 15142–15150 (2024).
27. Zhao, X. et al. Bioinspired ultra-stretchable and anti-freezing conductive hydrogel fibers with ordered and reversible polymer chain alignment. *Nat. Commun.* **9**, 3579 (2018).
28. Evertz, A., Schrein, D., Olsen, E., Hoffmann, G.-A. & Overmeyer, L. Dip coating of thin polymer optical fibers. *Opt. Fiber Technol.* **66**, 102638 (2021).
29. Mustafa Kamal, A., Misnon, M. I., Zakaria, M., Ab Kadir, M. & Ahmad, M. Characteristics of cotton, polyester and rayon fabrics coated with acetobacter xylinum. *Int. J. Eng. Technol.* **7**, 181–184 (2018).
30. Wang, B. et al. Synergistic modification of short-chain fluoro-alcohol and siloxane end-capping agents endowing an enhanced superhydrophobic waterborne polyurethane coating. *J. Appl. Polym. Sci.* **140**, e54250 (2023).
31. Wen, Z. et al. Recyclable EGaIn/TPU sheath–core fibres for superelastic electronics and sensing applications. *J. Mater. Chem. C.* **11**, 12163–12173 (2023).
32. Jia, Y. et al. Flexible and thin multifunctional waterborne polyurethane/Ag film for high-efficiency electromagnetic interference shielding, electro-thermal and strain sensing performances. *Compos. Part B: Eng.* **210**, 108668 (2021).
33. Chen, G. et al. Superelastic EGaIn composite fibers sustaining 500% tensile strain with superior electrical conductivity for wearable electronics. *ACS Appl. Mater. Interfaces* **12**, 6112–6118 (2020).
34. Zheng, L. et al. Conductance-stable liquid metal sheath-core microfibers for stretchy smart fabrics and self-powered sensing. *Sci. Adv.* **7**, eabg4041 (2021).
35. Zhang, Y. et al. Liquid metal enabled elastic conductive fibers for self-powered wearable sensors. *Adv. Mater. Technol.* **8**, 2202030 (2023).

36. Zhuang, Q. et al. Liquid–metal-superlyophilic and conductivity–strain-enhancing scaffold for permeable superelastic conductors. *Adv. Funct. Mater.* **31**, 2105587 (2021).
37. Wang, C. et al. Continuous meter-scale wet-spinning of cornlike composite fibers for eco-friendly multifunctional electronics. *ACS Appl. Mater. Interfaces* **13**, 40953–40963 (2021).
38. Lan, L., Jiang, C., Yao, Y., Ping, J. & Ying, Y. A stretchable and conductive fiber for multifunctional sensing and energy harvesting. *Nano Energy* **84**, 105954 (2021).
39. Sun, F. et al. Stretchable conductive fibers of ultrahigh tensile strain and stable conductance enabled by a worm-shaped graphene microlayer. *Nano Lett.* **19**, 6592–6599 (2019).
40. Zhou, J. et al. Buckled conductive polymer ribbons in elastomer channels as stretchable fiber conductor. *Adv. Funct. Mater.* **30**, 1907316 (2020).
41. Li, Y. et al. Ultrastretchable and wearable conductive multifilament enabled by buckled polypyrrole structure in parallel. *npj Flex. Electron* **6**, 42 (2022).
42. Lei, L., Xia, Z., Lin, X., Yang, T. & Zhong, L. Synthesis and adhesion properties of waterborne polyurethane dispersions with long-branched aliphatic chains. *J. Appl. Polymer Sci.* **132**, 41688 (2015).
43. Bao, L. et al. Effect of surface free energy and wettability on the adhesion property of waterborne polyurethane adhesive. *RSC Adv.* **6**, 99346–99352 (2016).
44. Kang, M. et al. Low-voltage organic transistor memory fiber with a nanograined organic ferroelectric film. *ACS Appl. Mater. Interfaces* **11**, 22575–22582 (2019).
45. Faustini, M., Louis, B., Albouy, P. A., Kuemmel, M. & Grosso, D. Preparation of sol−gel films by dip-coating in extreme conditions. *J. Phys. Chem. C.* **114**, 7637–7645 (2010).
46. Le Berre, M., Chen, Y. & Baigl, D. From convective assembly to Landau−Levich deposition of multilayered phospholipid films of controlled thickness. *Langmuir* **25**, 2554–2557 (2009).
47. Park, J.-E., Kang, H. S., Koo, M. & Park, C. Autonomous surface reconciliation of a liquid-metal conductor micropatterned on a deformable hydrogel. *Adv. Mater.* **32**, 2002178 (2020).
48. Li, R. et al. In situ identification of the metallic state of Ag nanoclusters in oxidative dispersion. *Nat. Commun.* **12**, 1406 (2021).
49. Yu, A. et al. Core–Shell-Yarn-Based triboelectric nanogenerator textiles as power cloths. *ACS Nano* **11**, 12764–12771 (2017).
50. Frey, E. J., Im, S., Bachmann, A. L., Genzer, J. & Dickey, M. D. Patterning of a high surface area liquid metal-carbon composite film using laser processing. *Adv. Funct. Mater.* **34**, 2308574 (2024).
51. Handschuh-Wang, S. et al. The liquid metal age: a transition from Hg to Ga. *Adv. Mater.* **36**, 2408466 (2024).
52. Ryu, S. et al. Light intensity-dependent variation in defect contributions to charge transport and recombination in a Planar MAPbI3 Perovskite solar cell. *Sci. Rep.* **9**, 19846 (2019).
53. Choi, B. et al. Highly conductive fiber with waterproof and self-cleaning properties for textile electronics. *ACS Appl. Mater. Interfaces* **10**, 36094–36101 (2018).
54. Martins, J. C., de, M., Neto, J. C., Passos, R. R. & Pocrifka, L. A. Electrochemical behavior of polyaniline: a study by electrochemical impedance spectroscopy (EIS) in low-frequency. *Solid State Ion.* **346**, 115198 (2020).
55. Zhao, Y. et al. Ultra-conformal skin electrodes with synergistically enhanced conductivity for long-time and low-motion artifact epidermal electrophysiology. *Nat. Commun.* **12**, 4880 (2021).
56. Hossain, M. M., Li, B. M., Sennik, B., Jur, J. S. & Bradford, P. D. Adhesive free, conformable and washable carbon nanotube fabric electrodes for biosensing. *npj Flex. Electron* **6**, 1–9 (2022).

Acknowledgements

This research was funded by the Ministry of Science and ICT (MSIT) (Grant No. IITP-2023-2020-0-01461, RS-2023-00213089, RS-2024-00403639, RS-2024-00403163). This research was funded by the Ministry of Trade, Industry and Energy (MOTIE) (Grant No. P0017805, RS-2022-00154781). This work was funded by the Ministry of Education (MOE) (Grant No. RS-2023-00220077).

Author contributions

H.K. fabricated the CTFs, performed electrical and microscopic data analysis, and took the lead in drafting and writing the manuscript. J.-G.C. analyzed the XPS results and made significant contributions to revising and refining the manuscript. T.O., I.L., and H.L. supported experiments, involving waterproofing and washability tests. H.J. and C.-H.H. supported microscopic data analysis. H.J.K. analyzed the physiological signal data, including ECG and EMG signal processing, and contributed to the interpretation of results under wet and washing conditions. T.-W.K. contributed to the development and optimization of the CTAC process, ensuring efficient and scalable production of the fibers. S.P. conceived the research concept, secured funding, and supervised the project, providing guidance throughout its development and ensuring its successful completion. All authors contributed to the discussion on the manuscript.

Competing interests

The authors declare no competing interests.

Ethics declarations

The participant in the biosignal sensing experiments was a co-author of this work and provided informed consent.

Additional information

Supplementary information The online version contains supplementary material available at https://doi.org/10.1038/s41528-025-00399-3.

Correspondence and requests for materials should be addressed to Hye Jin Kim, Tae-Wook Kim or Sungjun Park.